Research Article | Vol. 27, No. 20 / 30 September 2019 / Optics Express 28692
Optics EXPRESS

Zernike mapping of optimum dwell time in deterministic fabrication of freeform optics

WULE ZHU AND ANTHONY BEAUCAMP*

Department of Micro-Engineering, Kyoto University, 615-8510, Kyoto, Japan
**beaucamp@me.kyoto-u.ac.jp*

Abstract: In optics fabrication technologies such as computer controlled optical surfacing (CCOS), accurate computation of the dwell time map plays an essential role in the deterministic performance of the fabrication process. However, it is still difficult for existing methods to derive smooth dwell time maps that reduce dynamic stressing on the machine especially at the aperture edge region, while retaining fine correction capability on freeform optics. To answer these challenges, we propose a new method based on Zernike decomposition and improved differential evolution optimization of the dwell time map, which can be applied to time-dependent optics fabrication processes such as fluid jet machining. Simulations and experiments based on a bi-sinusoidal freeform design were carried out to assess the feasibility of the proposed methodology. With appropriate fluid jet pressure, a bi-sinusoidal optical surface with demanding form error target of sub-100 nm in peak-to-valley was achieved, showing a remarkable improvement on the state-of-the-art, while keeping a good average surface roughness of 2.6 nm Ra on the optical glass.

1. Introduction

In recent years, there has been a rapidly increasing demand for an ever wider array of advanced optical systems, resulting in a strong need for accurate and efficient manufacturing of optics with complex shapes, especially freeforms [1]. Diamond tool based single point cutting is a deterministic optics fabrication method that can generate freeform optics with surface roughness of 5~10 nm Ra [2], but it highly relies on the positioning accuracy of the machine and sharpness of the cutting tool [3]. Besides, diamond turning marks are unavoidable, and surface fracture can be easily induced when processing brittle material such as glass or ceramics. Hence, various computer-controlled optical surfacing (CCOS) methods have been developed over the past decades including magnetorheological finishing [4], elastic emission machining [5], fluid jet polishing [6], bonnet polishing [7], etc.

Among these, fluid jet polishing consists of pressurized slurry passing through a nozzle and removing materials by impingement of the workpiece, and is considered a versatile process for super fine finishing of small and complex components [8,9]. It possesses a number of merits including: 1) absence of tool wear and edge effect due to the non-contact removal mechanism, 2) ability to generate submillimeter removal footprint that adapt to complex surfaces. Owing to these advantages, super fine finish without residual tool marks can be achieved when post-processing diamond turned surfaces such as X-ray molding dies [10]. Nonetheless, this technology could bring higher added-value in industry if it could be applied to direct fabrication of freeform optical surfaces with ultraprecise form error (peak-to-valley < 100 nm) in a fully automated and deterministic manner, rather than mere post-polishing.

As a CCOS method, the fluid jet scan feed can be controlled to produce "equivalent dwell" at discrete positions of the workpiece. The resulting material removal map can be computed by 2D convolution of the dwell time map and removal footprint (termed here as the influence function). Hence, reverse calculation of dwell time is a deconvolution problem that greatly influences the ability of realizing highly detailed and accurate surfaces. To remove residual form error, previous

#371375 https://doi.org/10.1364/OE.27.028692
Journal © 2019 Received 1 Jul 2019; revised 31 Jul 2019; accepted 31 Jul 2019; published 23 Sep 2019

Optics EXPRESS

researches have proposed several methods to compute dwell time for CCOS methods. According to literature review, the most popular algorithms for solving the dwell time are the convolution iterative method and Fourier transform [11]. The convolution iterative method proposed by Jones et al. [12] is based on the 2D convolution algorithm and a computation loop for updating dwell time. This method has fast computation speed but limited accuracy and convergence rate, sometimes even failing to converge [13]. To avoid divergence, a damping factor can be introduced when updating dwell time for the next iteration. However, the factor is not constant and varies case-by-case, making the method difficult to harness for the average user. A modified version with self-adaptive damping factor was proposed, and realized a high convergence ratio and fast solution speed for large aperture optics according to their simulation [14]. As the second main type of solving algorithm, the Fourier transform method converts the 2D convolution process into a product problem in frequency domain [15]. However, negative dwell time are usually generated by this method, and computation can again fail to converge to a satisfactory solution.

In another commonly used approach, the discrete convolution is transferred to a linear equation model [16], namely $\boldsymbol{Ax} = \boldsymbol{b}$, and the dwell time vector $\boldsymbol{x}$ is obtained through least-squares (LSQR) algorithm. Basically, this method describes the removal footprint and tool path in a large coefficient matrix $\boldsymbol{A}$ with rows equal to the total number of observation points in the surface error matrix $\boldsymbol{b}$ and columns equal to the number of tool path points [17]. Because $\boldsymbol{A}$ is usually large scaled and ill-posed with a large condition number, Tikhonov regularization has been adopted to obtain a stable solution [18]. Based on this method, a damping factor was also introduced to obtain a high convergence rate [19]. Nevertheless, the computation load is very large and the damping factor remains unfixed depending on the tool path and the target to achieve. Experience indicates that a small factor results in a small residual error in the central region while causing a remarkably large error at the edge, which leads to a smaller clear aperture for the produced optical components in practice. Considering this kind of edge problem is induced in optimization by conventional deconvolution algorithm, the inclusion of an extra marginal factor was attempted to control the edge accuracy [11]. Besides, with a small damping factor, serious oscillation is generated on the dwell time map, which poses a huge mechanical burden for the polishing machine and challenges the machine dynamics. This is because the high-frequency component of dwell time map leads to high-frequency variation in feed velocities [17], acceleration and jerk, thus imposing dynamic restrictions on the machine tool [20]. On the contrary, a large damping factor contributes to a smooth but very large residual error which means this method is rarely the best approach. From the above literature review, it is clear that a better approach is needed to derive optimum solutions of dwell time, that does not over burden the machine and keeps high fidelity at the edge, for deterministically fabricating freeform optics on brittle materials such as optical glass or ceramics.

Zernike polynomials are a popular tool to analyze the aberration in the design procedure of freeform optics [21,22]. In this study, Zernike polynomials are innovatively utilized in the fabrication stage to generate freeform optics. Specifically, from a starting potential dwell time map based on the formulated volumetric removal rate and Zernike decomposition, a differential evolution algorithm is then adopted to find the optimum dwell time map by adjusting each order of Zernike polynomial with the target of achieving the minimum residual error. Since the mapped Zernike dwell time possesses freeform features, it is evenly smooth over the entire area without high-frequency oscillation or steep steps. Consequently, it is very advantageous for the machine as feeds are smooth. The significantly large error at the edge region observed in the general LSQR method with damping factor can be completely eliminated. Besides, fast convergence rate with residual error below 100 nm PV can be achieved with the new approach.

Optics EXPRESS

2. Methodology for Zernike mapping of optimum dwell time

2.1. DFJ principle

The basic principle of deterministic fluid jet (DFJ) fabrication is to utilize high pressure fluid jet to fabricate the optical workpiece in ductile mode and remove materials in a deterministic manner so as to obtain a super finished surface. In specific, fluid jet mixed with water and abrasive particles is delivered from a pump to a converging nozzle of outlet diameter in the range of 0.1~2.0 mm [10]. When impinging a static location, the fluid jet generates a concave spot termed as influence function, as shown in Fig. 1(a). Typically, the fluid jet head is clamped on a robot arm to achieve flexibility in aligning with the workpiece normal vector, whilst the optical workpiece contours are followed with translational axes of the machine. In a dynamic situation, as the influence function with center point P (i, j) moves along a designated trajectory that is discretized by the black points shown in Fig. 1(b), the surrounding material is removed. Mathematically, the removal amount is the convolution of the jet influence function and equivalent dwell time at the corresponding discrete locations. Given the target of a freeform shape to be machined, an optimum set of dwell times for these discrete points needs to be determined.

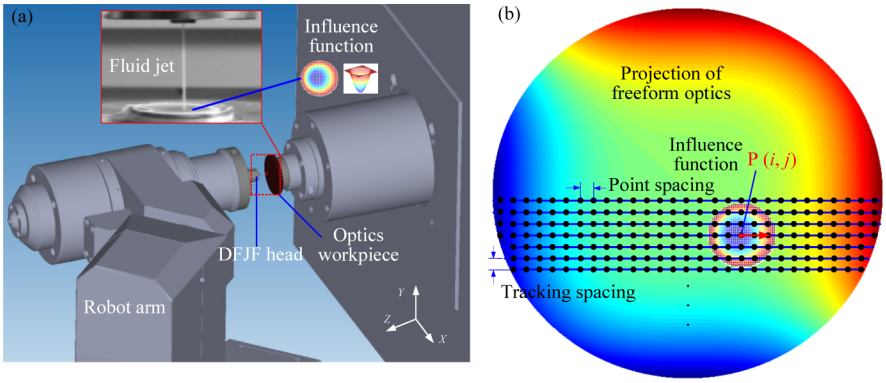

Fig. 1. (a) Principle of fluid jet fabrication, (b) illustration of material removal based on influence function.

2.2. Zernike mapping method

Due to its rotationally symmetric aspect, the influence function generated with a nozzle smaller than 0.5 mm diameter can be well described by a Gaussian distribution in the influencing area of fluid jet, namely:

$$Z_{\text{inf}}(w_{xy} \cdot x, w_{xy} \cdot y) = w_A \cdot A \cdot e^{\frac{-(x^2+y^2)}{B}} \tag{1}$$

where $x, y \in [-R_{\text{inf}}, R_{\text{inf}}]$; The coefficient A determines the removal depth, and B is related to the spot width of the influence function. In addition, w_{xy} and w_A are scale factors that are used in this study to adjust the influence area and removal depth, respectively.

With the identified influence function, the conventional LSQR method with damping factor has been widely used to calculate the dwell time [19,23]. However, to achieve a sufficiently small residual error, the derived dwell time map has the same level of smoothness as the removal map over the target area and generates especially large error at edges. In our approach, the starting initial dwell time map is derived from the volumetric removal rate (*VRR*), which inherits smooth

Optics EXPRESS

features in the case of freeform surfaces without steps, since it can be practically determined by:

$$t_d^{VRR} = (ZT \cdot \Delta x \cdot \Delta y)/VRR \tag{2}$$

$$VRR = \frac{1}{t_d}\int_0^{t_d}(\iint \frac{\partial Z_{\inf}}{\partial t}dxdy)dt \tag{3}$$

where ZT is the removal height of freeform optical surface at position (XT, YT); t_d is the dwell time of static influence function; Δx and Δy are the point spacing and track spacing, respectively, as shown in Fig. 1(b).

According to the Preston law, VRR is proportional to $P{\cdot}V$ where P is the pressure in the area of influence function and V is the velocity of abrasive particle. In DFJ process, the pressure P of fluid jet is inherently coupled with the velocity V through the Bernoulli equation. In theory, the dynamic pressure of fluid is proportional to the square of velocity. Based on this, the VRR of DFJ can be expressed in the following form:

$$VRR = k_0 PV = k_p(P - P_0)^m \tag{4}$$

where k_0 is the Preston constant; k_p and m are coefficients that need to be identified. P_0 is the threshold pressure to initiate material removal.

The VRR based dwell time derivation features a typical smoothness equivalent to that of the target freeform profile, which is beneficial to keeping within machine dynamic characteristics like maximum acceleration and jerk properties. According to our experience, this method is capable of converging form error with a spatial content larger than the influence spot width, but struggles to reach below 100 nm peak-to-valley (PV) due to small fluctuations in pre-processing characteristics (instant jet pressure and abrasives density) that typically leave a signature with spatial content smaller than the influence spot. With the VRR based dwell time as the starting basis, the new approach with adjustable Zernike terms is to further optimize dwell time to achieve as minimum residual form error as possible.

According to Eq. (2), the dwell time ${t_d}^{VRR}$ at location (XT, YT) is proportional to the freeform target ZT. Therefore, it can be approximated with Zernike polynomials that are mathematically decomposed in the following form:

$$t_d^{VRR} = \sum\nolimits_{m,\,n}[a_{m,\,n} \cdot Z_n^m(\rho,\varphi) + b_{m,\,n} \cdot Z_n^{-m}(\rho,\varphi)] \tag{5}$$

where m and n are integers; The number of Zernike terms, namely the index number j according to OSA/ANSI [24], is $[n(n+2)+m]/2$; φ is the azimuthal angle, ρ is the radial distance in unit area (normalized as $0< \rho <1$); According to the definition, even and odd Zernike terms are expressed by:

$$Z_n^m(\rho,\varphi) = R_n^m(\rho) \cdot cos(m\varphi) \tag{6}$$

$$Z_n^{-m}(\rho,\varphi) = R_n^m(\rho) \cdot \sin(m\varphi) \tag{7}$$

where the radial polynomials are defined as:

$$R_n^m(\rho) = \sum\nolimits_{k=0}^{\frac{n-m}{2}} \frac{(-1)^k \cdot (n-k)!}{k! \cdot (\frac{n-m}{2}-k)! \cdot (\frac{n+m}{2}-k)!} \cdot \rho^{n-2k} \tag{8}$$

Due to the orthogonal property of Zernike polynomials in unit area, the coefficients in Eq. (5) can be expressed as follows:

$$a_{m,\,n} = \frac{2n+2}{\varepsilon_m \pi}\int t_d^{VRR}(\rho,\varphi) \cdot Z_n^m(\rho,\varphi)\rho d\rho d\varphi \tag{9}$$

$$b_{m,\,n} = \frac{2n+2}{\varepsilon_m \pi}\int t_d^{VRR}(\rho,\varphi) \cdot Z_n^{-m}(\rho,\varphi)\rho d\rho d\varphi \tag{10}$$

where ε_m=2 if m = 0, otherwise is 1.

Optics EXPRESS

Consequently, the dwell time ${t_d}^{VRR}$ can be initially approximated at the first step ($i = 0$) by substituting Eqs. (6-10) into Eq. (5), and with the addition of adjustable coefficients to the polynomials. The evolved dwell time at any step i is given by:

$$ {}^{i}t_d^{ZK} = \sum\nolimits_{m,\,n} [ka^{i}_{m,\,n} \cdot a_{m,\,n} \cdot Z_n^m(\rho, \varphi) + kb^{i}_{m,\,n} \cdot b_{m,\,n} \cdot Z_n^{-m}(\rho, \varphi)] \tag{11} $$

where ${ka_{m,\,n}}^{i}$ and ${kb_{m,\,n}}^{i}$ are the adjustable coefficients to be optimized; For the first step $i = 0$, ${}^{0}{t_d}^{ZK} = {t_d}^{VRR}$ as the initial values are ${kb_{m,\,n}}^{0} = \mathrm{kb}_{m,\,n}{}^{0} = 1$.

With the dwell time ${}^{i}{t_d}^{ZK}$ at the i^{th} step, the material removal can be computed by forward convolution as:

$$ \begin{bmatrix} F(h_1, N_2) & & & \\ F(h_2, N_2) & F(h_1, N_2) & & \\ \vdots & F(h_2, N_2) & \ddots & \\ F(h_{M1}, N_2) & \vdots & \ddots & F(h_1, N_2) \\ & F(h_{M1}, N_2) & & F(h_2, N_2) \\ & & & \\ & & & F(h_{M1}, N_2) \end{bmatrix} \begin{bmatrix} {}^{i}t_{d_0}^{ZK} \\ {}^{i}t_{d_1}^{ZK} \\ \\ {}^{i}t_{d_{N_1 \cdot N_2 - 1}}^{ZK} \end{bmatrix} = Z \tag{12} $$

where h_l is the l^{th} row of influence function Z_{inf} (x, y) which is sampled based on the discrete points shown in Fig. 1(b). Hence, its size is (M_1, M_2)=(R_{inf} /Δx, R_{inf} /Δy). The size of dwell time vector ${}^{i}{t_d}^{ZK}$ is (N_1, N_2)=(R/Δx, R/Δy) where R is the aperture radius of optical workpiece. The first matrix on the left of equation is a 2D convolution kernel matrix with N_1 matrix columns and N_2 columns in each submatrix $F(h_1, N_2)$ which is constructed by 1D convolution kernel [11].

Thus, the total size of the expansion matrix in Eq. (12) is ((N_1+M_1−1)*(N_2+M_2−1), N_1*N_2), and the size of convolution result Z is ((N_1+M_1−1)*(N_2+M_2−1), 1). Note that its size is larger than the size of freeform target ZT due to the dwell of influence function at the edge region. By reshaping Z to (N_1+M_1−1, N_2+M_2−1) and cropping to the same size as ZT, namely (N_1, N_2), the convolution result ${}^{i}{ZT}^{ZK}$ of removal in the freeform target area for the i^{th} step of the evolved dwell time ${}^{i}{t_d}^{ZK}$ can be obtained.

2.3. Differential evolution optimization

To find the optimum dwell time, the result of i^{th} step is derived from the (i-1)$^{\text{th}}$ step, by means of improved differential evolution optimization algorithm, which is an efficient evolutionary optimization algorithm motivated by natural selection [25]. To achieve this, the adjustable coefficients ${ka_{m,\,n}}^{i}$ and ${kb_{m,\,n}}^{i}$ that determine the proportion of (m, n) Zernike polynomials are regarded as the population, the total number of which is equal to the Zernike index number j. For each population, its size is chosen as M. During the optimization process, the value of every individual in each population is experienced within the designated range [k_s, k_e]. Initially, for the first generation $i = 0$ values are selected randomly within the range. As the generations proceed, new individual values are generated through mutation operation and cross over (mimicking natural selection). The best individuals are selected from the population at the i^{th} generation, on the basis of minimum residual error within the area of interest. Thus, compared with the target freeform surface, the cost function is defined as:

$$ Obj = min\{||(XT, YT, ZT) - (XT, YT, {}^{i}{ZT}^{ZK})||^2\} \tag{13} $$

where || || is the Euler operator, describing the distance between optimized and target surface profiles.

Optics EXPRESS

On condition that the generation reaches the maximum number G, the best individual values are selected as $ka_{m,n}{}^{G}$ and $kb_{m,n}{}^{G}$. By substituting into Eq. (11), the optimum dwell time ${}^{G}t_d{}^{ZK}$ for all locations (XT, YT) can be finally obtained. With the optimized Zernike based dwell time map, any arbitrary machining path can be planned [26], as long as it goes through all the sampled discrete points without repetition. This is because the dwell time map is smooth and continuous over the entire target surface.

3. Simulation and validation

Simulations were conducted to validate the feasibility and advantages of the proposed approach. The flowchart of the Zernike based optimization process of dwell map is shown in Fig. 2, and summarized by the following steps:

- Given the freeform surface target (XT, YT, ZT), the initial dwell time map is calculated from Eq. (2) and the volumetric removal rate predicted by Eqs. (3-4) using process parameters, especially pressure (Eq. 4).
- Zernike decomposition of the obtained initial dwell time map is performed, serving as the 0^{th} generation of dwell time map (${}^{0}t_d{}^{ZK}$ by Eq. 5) before executing the optimization process.
- The 1^{st} generation of dwell time map is constructed by setting the coefficients ($ka_{m,n}{}^{i}$ and $kb_{m,n}{}^{i}$) of Zernike terms as initial random numbers within the range [k_s, k_e].
- Forward convolution is carried out between the influence function and dwell time map along the path trajectory, and the results are given by (XT, YT, ${}^{i}t_d{}^{ZK}$) through Eq. 12. Residual error is calculated (Eq. 13) by registering with the designed freeform target.
- Differential evolution optimization is carried out to update the Zernike dwell time map until residual error satisfies the tolerance, or maximum number of generation is reached. The optimum Zernike dwell time map is finally obtained as (XT, YT, ${}^{j}t_d{}^{ZK}$), where $j \le G$.

As proof of concept, the simulated removal target is a freeform bi-sinusoidal surface on optical glass typically used for 2D optical encoder application [27], expressed as:

$$ZT = A_m \cdot [\cos(\frac{2\pi}{\lambda} \cdot XT) + \cos(\frac{2\pi}{\lambda} \cdot YT)] - A_0 \tag{14}$$

where $x^2+y^2 \le 6.25^2$; A_m is the amplitude coefficient, and A_0 is a bulk removal offset. λ is the wavelength of the pattern. In this specific case, A_m=0.1 μm, A_0=0.7 μm, and λ=5 mm. The parameters of influence function expressed in Eq. (1) are set as $A = 0.03$, $B = 1$. A raster path is adopted with point spacing of 0.2 mm and track spacing of 0.05 mm. In fabricating this freeform surface with PV amplitude of 0.4 μm according to Eq. (14), the target residual error is sub-100 nm in PV, and below 5 nm in root-mean-square (RMS).

The maximum number of generation G is set to a high value of 200, to guarantee full convergence. The index number j of Zernike terms is 200. Therefore, the number of population is 200, and the size of each population, G, is 60. The optimization range for each individual $ka_{m,n}{}^{i}$ or $kb_{m,n}{}^{i}$ is [0.2, 5], which means the evolved coefficients will be between 0.2 and 5 times the initial coefficient value of 1. This range was established through trial and error in the initial stage, so as to maximize convergence while avoiding unnecessary calculation steps. By executing the above flowchart, the convergence curve of the objective function (Eq.13) with respect to the generation number is plotted in Fig. 3(a). It can be seen that the objective quickly converges within 50 generations with the value dropping from $3e^{-6}$ to $0.1e^{-6}$, indicating that the proposed framework for dwell time optimization is functioning correctly. After 200 generations,

Optics EXPRESS

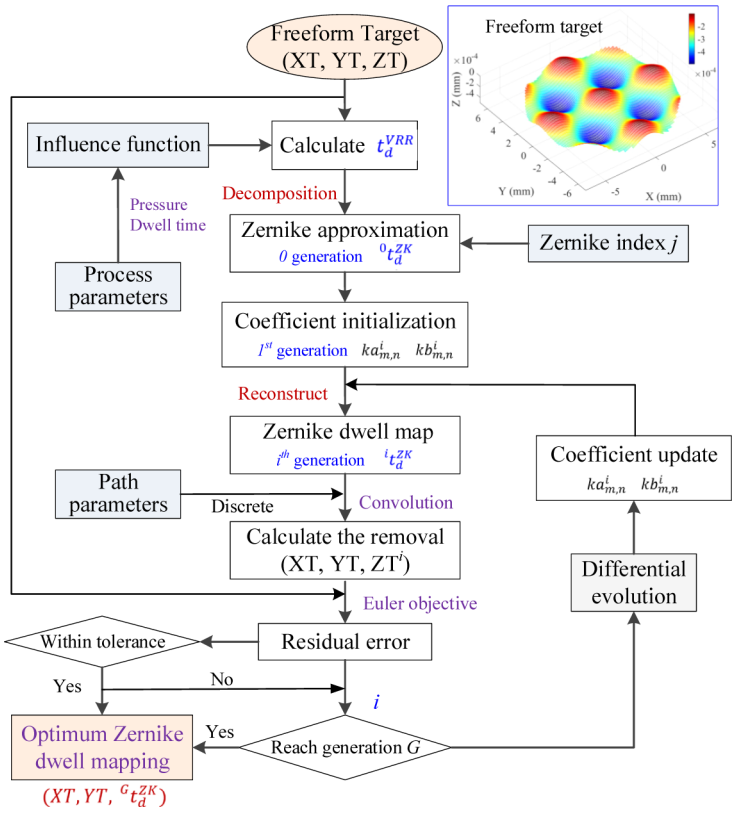

Fig. 2. Flowchart of Zernike based dwell map optimization for freeform optics generation.

the coefficients of Zernike terms $ka_{m,n}{}^i$ and $kb_{m,n}{}^i$ are finally obtained and plotted in Fig. 3(b), where the Zernike index is $j = [n(n+2)+m]/2$. Wide variations compared with the initial value of 1 can be noticed.

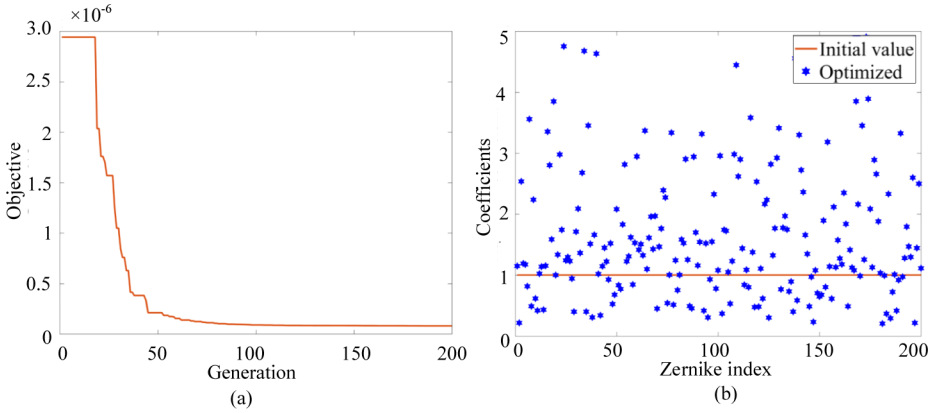

Fig. 3. (a) Convergence of objective cost function, (b) Optimized coefficients of Zernike terms.

The evolution of residual error with respect to the generation number is evaluated in Fig. 4. For the 0th generation (*VRR* method, before optimization), the PV value of the residual error is

Optics EXPRESS

66 nm, with a sinusoidal shape clearly resembling the removal target, albeit on a smaller scale. The RMS value is calculated to be 34 nm. At 1st generation, the residual error becomes irregular since the coefficients of Zernike terms are randomly selected. Nonetheless, after 25 generations of the optimization, the PV value of residual error has been improved by 5 folds, evidence of which can be also found in the convergence curve in Fig. 3(a). The RMS value is significantly lowered to 2.3 nm accordingly. The residual error further reduces at 50 generations, and seems to remain stable afterwards. At 200 generations, the residual error has been significantly minimized to 12 nm in PV, as shown in Fig. 4.

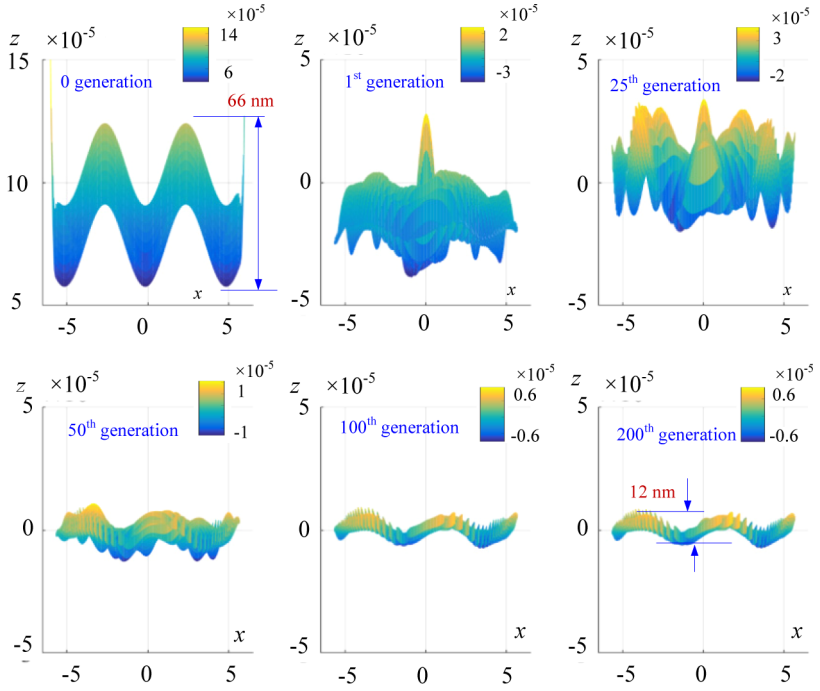

Fig. 4. The evolution of residual error with respect to generation number (axis units: mm).

The results of *VRR* method (before optimization), Zernike mapping optimization method, and conventional iterative method (LSQR) are compared in Fig. 5, showing 3D and side views of the result for each method. It can be seen that the *VRR* method results in a large form error everywhere, while the conventional iterative method is able to minimize form error only in the central region. A significantly larger error is formed close to the edge region, especially when using a small damping factor as recommended in the literature. The corresponding RMS value is characterized to be 16 nm. In addition, profiles through the workpiece center along X direction were extracted from the three different dwell time maps, as plotted in Fig. 6(a). It can be found that the LSQR dwell time wildly fluctuates as compared to the Zernike mapping method and VRR method. Based on the discrete differential method, the corresponding feed velocities can be accordingly obtained in Fig. 6(b). It shows significantly high feeds for the LSQR method, which can lead to high dynamics when evaluating the acceleration and jerk (differential of acceleration) as shown in Fig. 6(c) and (d), respectively. General LSQR method generates significantly higher acceleration and jerk, which cannot be attained due to automated filtering by the controller to stay within the dynamic envelope of the machine. In the VRR method and Zernike mapping method these problems can be avoided, though the new Zernike approach possesses advantages of both

Optics EXPRESS

VRR method and LSQR method in achieving minimum residual error together with moderate machine feed fluctuations.

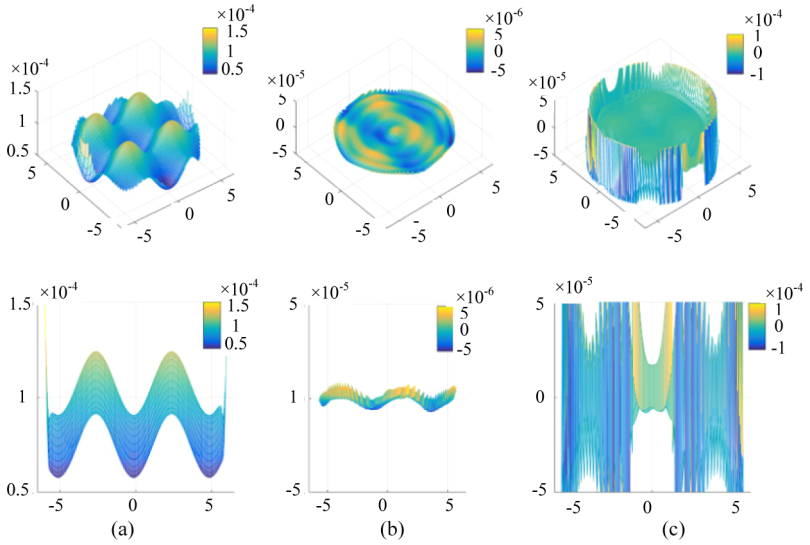

Fig. 5. Residual errors after dwell time computation by (a) VRR based approach, (b) Zernike mapping optimization, (c) conventional iterative calculation (axis units: mm)

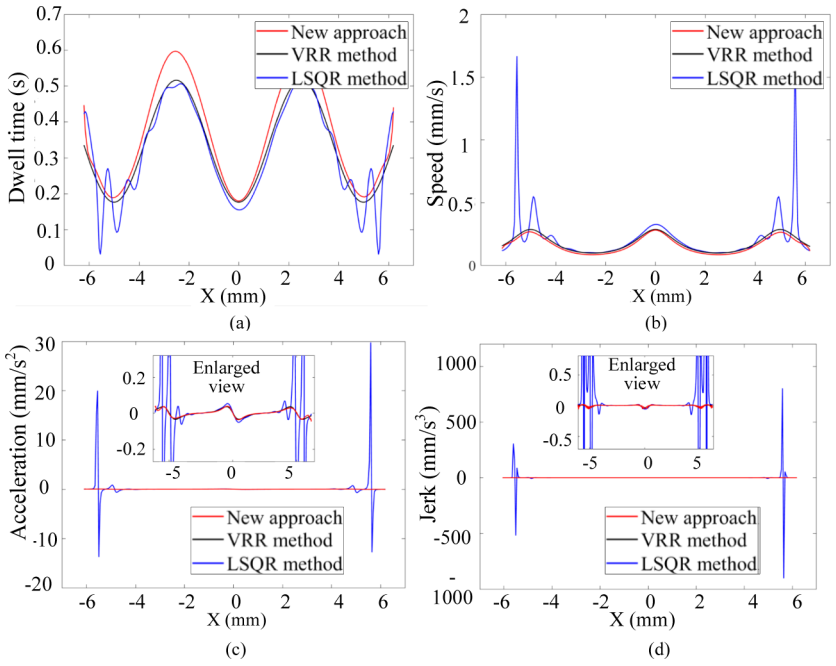

Fig. 6. (a) Dwell time profiles, (b) velocities, (c) acceleration, (d) jerk performances by three methods through the workpiece center.

To demonstrate applicability of the proposed approach for different conditions of influence function, RMS value of the residual error was investigated with respect to the removal rate and

Optics EXPRESS

width of influence function, which are the two dominant characteristics in the DFJ process. When the scale factor w_A that determines the removal rate of influence function in Eq. 1 is applied, the RMS value of the corresponding residual form error is evaluated as shown in Fig. 7(a). The small deviation of results around the average of 2.4 nm in RMS indicates that residual error does not depend much on the removal rate of the influence function. By keeping w_A=1 but varying the width factor w_{xy}, the RMS value is also found to not dependent much on the width of influence function either. However, it is noted that convergence speed is faster for larger width of influence function. Building on these observations, high outlet pressure from the nozzle and larger nozzle size can be applied to achieve equal level of accuracy in residual form error as conditions that are more benign. However, the selection of process parameters may compromise the achievable surface roughness quality, so an investigation of this aspect is included in the following section.

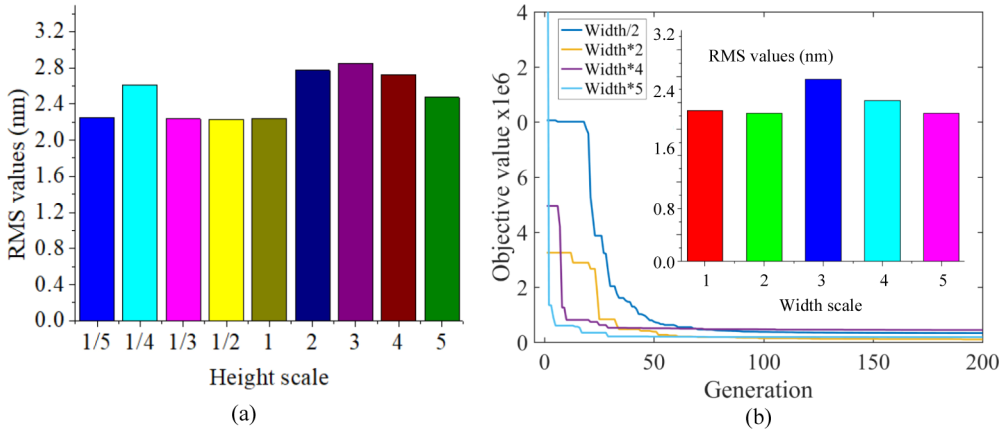

Fig. 7. RMS error with respect to (a) removal rate and (b) width of influence function.

4. Experimental demonstration

4.1. Setup

Experimental validation was carried out on a 7-axis machine (IRP200, Zeeko Ltd), as shown in Fig. 8. The fluid jet head is perpendicular to the workpiece surface, the outlet of which is set 2 mm away from the workpiece. The nozzle diameter is 0.25 mm. The adopted pressure in experiments varies from 4 Bar to 16 Bar. The workpiece is an optical plano (material: BK7, flatness $\lambda/4$). The slurry is a mix of pure water and Cerium oxide with 1.5 µm grit size and concentration of 20 g/L. The surface form before and after polishing was measured by Fizeau interferometer (Wyko NT4100) and the surface roughness was evaluated by white light interferometer (Wyko NT2000). The experimental process parameters are shown in Table 1.

Table 1. Experimental process parameters

Fluid Jet Pressure	4, 8, 12, 16 Bar	Track spacing	0.05 mm	Abrasives	CeO_2
Nozzle diameter	0.25 mm	Point spacing	0.2 mm	Particle size	1.5 µm
Workpiece	BK7 glass	Max feed velocity	100 mm/min	Concentration	20 g/L
Aperture diameter	12.5 mm	Nozzle offset	−2 mm		

Optics EXPRESS

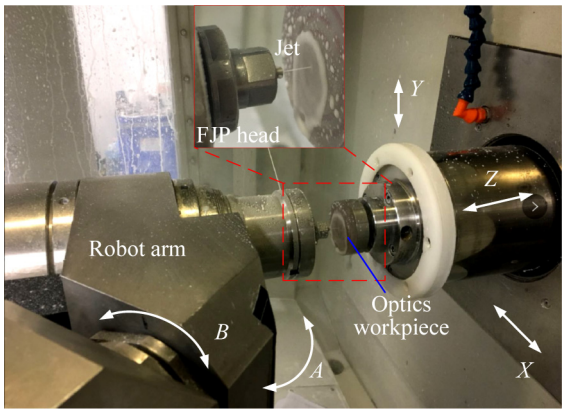

Fig. 8. Experimental setup for fluid jet fabrication of freeform optics.

4.2. Process investigation and parameter selection

Firstly, the effect of process parameter was investigated for parametric determination, by generating influence functions and raster machining of small regions. The adopted fluid jet pressures are 4 Bar, 8 Bar, 12 Bar and 16 Bar, with dwell time of 40 s, 20 s, 10 s and 10 s, respectively. The dwell time was selected so as to obtain a measurable depth of influence function by Fizeau interferometer, which is then normalized to *VRR*. The generated influence functions are plotted in the first row of Fig. 9, showing an increasing trend in removal depth as function of pressure. Using the four pressures, raster machining in small regions of 4 mm × 4 mm was performed for 40 s each, and the corresponding removal maps are shown in the second row of Fig. 9. By comparison, it can be found that removal under pressure of 4 Bar is negligible, and deepest under pressure of 16 Bar. Measurement and characterization of surface roughness are shown in the third row of Fig. 9. A smooth surface can be obtained below 12 Bar, whereas some waviness tends to appear at 16 Bar.

Based on these tests, trends for volumetric removal rate (*VRR*) and achievable surface quality are shown in Fig. 10. The *VRR* values are calculated by Eq. (3), and experimental data matches very well with the trend predicted from Eq. (4), where the coefficients k_p and m are identified as $2.27e^{-6}$ and 2.21 through best fit, and the threshold pressure P_0 is 4 Bar. Surface quality was evaluated by characterizing the roughness. For each pressure, five sample locations in the small polished region (Fig. 9) were measured. The surface roughness with error bar is plotted in terms of fluid jet pressure, as shown in Fig. 10(b). A more or less linearly increasing trend in surface roughness with pressure can be observed. However, it is noteworthy that the surface roughness at 12 bar is not much worse than compared with that at 8 bar, while *VRR* at that pressure is significantly higher. At 16 bar, although highest *VRR* can be obtained, some waviness (Fig. 9) was observed which contributes to the larger surface roughness value. Consequently, by considering both the machining efficiency and surface quality, 12 bar was selected as a reasonable pressure parameter for generation of freeform optics, as will be presented in the following section.

4.3. Deterministic fabrication of freeform optics

In this section, a typical bi-sinusoidal freeform optical surface with the same parameters as in Eq. 14 was machined experimentally on glass (BK7 material) with radius of 6.5 mm. A raster path was planned with point spacing Δx of 0.2 mm and track spacing Δy of 0.05 mm, as shown in Fig. 11(a). The fluid jet pressure was set to 12 Bar, and the same slurry as used in section 4.2 was adopted. Based on the proposed approach, the optimum Zernike dwell time map (*XT*, *YT*,

Optics EXPRESS

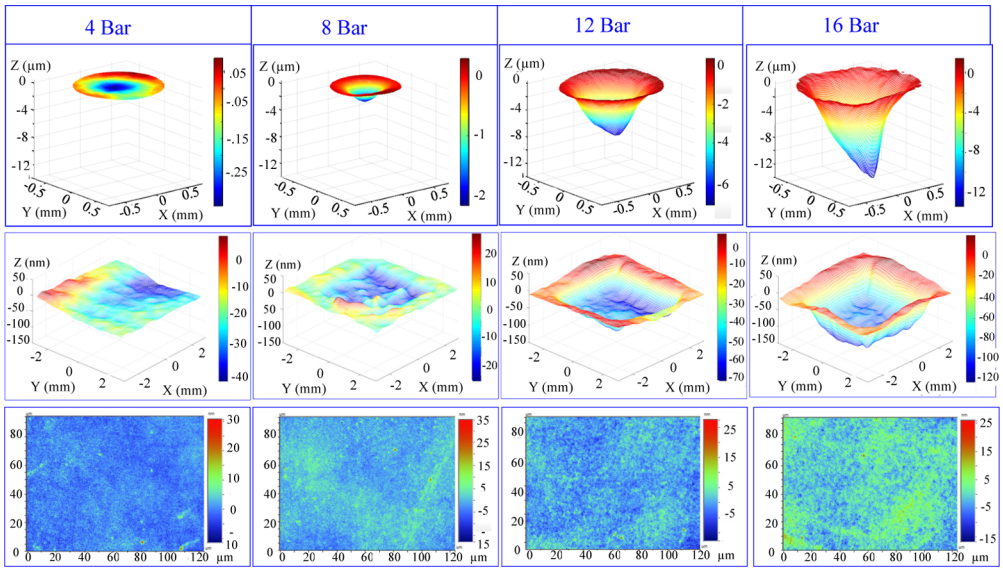

Fig. 9. Influence functions (1st row), planar removal (2nd row) and surface roughness (3rd row) under different fluid jet pressures.

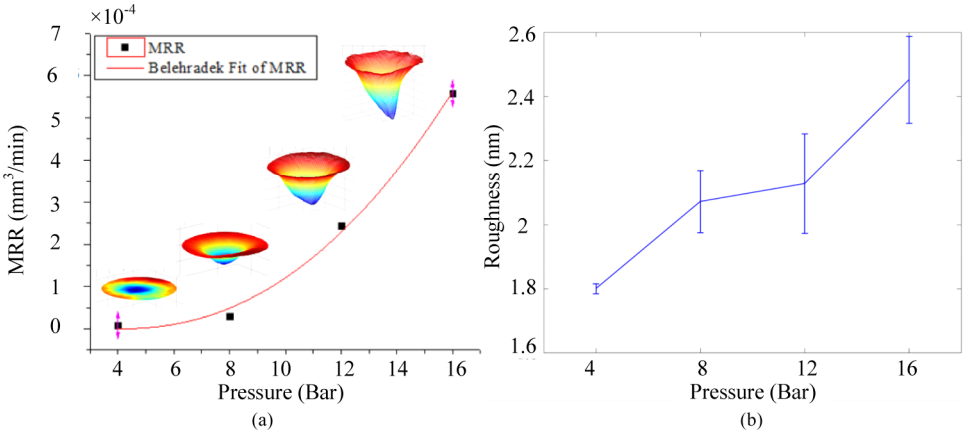

Fig. 10. (a) Volume removal rate (*VRR*), and (b) surface roughness under different pressures.

${}^{G}t_d{}^{ZK}$) was computed. Then, feed velocity along the path was moderated to be consistent with dwell time mapping, which can be expressed by (XT, YT, $\Delta x/{}^{G}t_d{}^{ZK}$). The corresponding feed velocity moderation along x-axis of the machine (direction of blue arrow in Fig. 11(a)) is drawn in Fig. 11(b). The total machining time is about 2 hours.

Freeform optical surfaces were machined according to both *VRR* method and the proposed approach. The resulting surface forms were measured by Fizeau interferometer. Although it has very high nominal accuracy, minor uncertainty exists between each measurement because of random variations such as noise, external vibration, etc. Based on a statistical evaluation of single measurements for the adopted interferometer, the discrepancy in PV for the fabricated bi-sinusoidal surface is basically around ± 5 nm. However, when measuring surface form by Fizeau interferometer, standard deviation of the PV can be reduced to less than 1 nm by taking the average of multiple measurements [28]. Consequently, the final measured surface forms

Optics EXPRESS

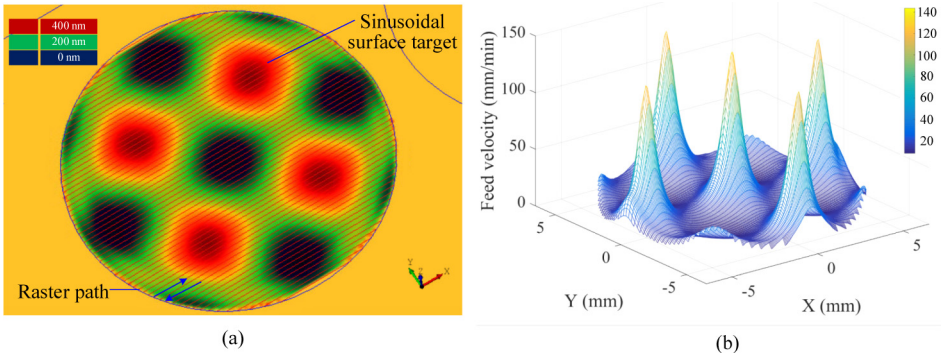

Fig. 11. (a) Raster path planning for freeform surface generation, (b) Moderation of feed velocity based on optimized Zernike dwell time map.

shown in Fig. 12(a) and 12(b) were obtained by taking 8 measurements and averaging in the software, which provides sufficient accuracy for comparative analysis of the fabricated surfaces using different methods. After best-fit 3D spatial registration with the ideal bi-sinusoidal surface, residual form error of the *VRR* method is shown in Fig. 12(c). The residual form error inherent to VRR can be clearly seen to agree with the prediction in Fig. 4. The PV value of this residual error is evaluated to be about 150 nm. By comparison, in case of the Zernike mapping constructed by the new approach after 200 generations, the residual form error is significantly reduced and characterized to be only ± 28 nm in the central region. The slightly larger form error at one side of the region is considered to be caused by drift of the fluid jet pressure, as it was controlled

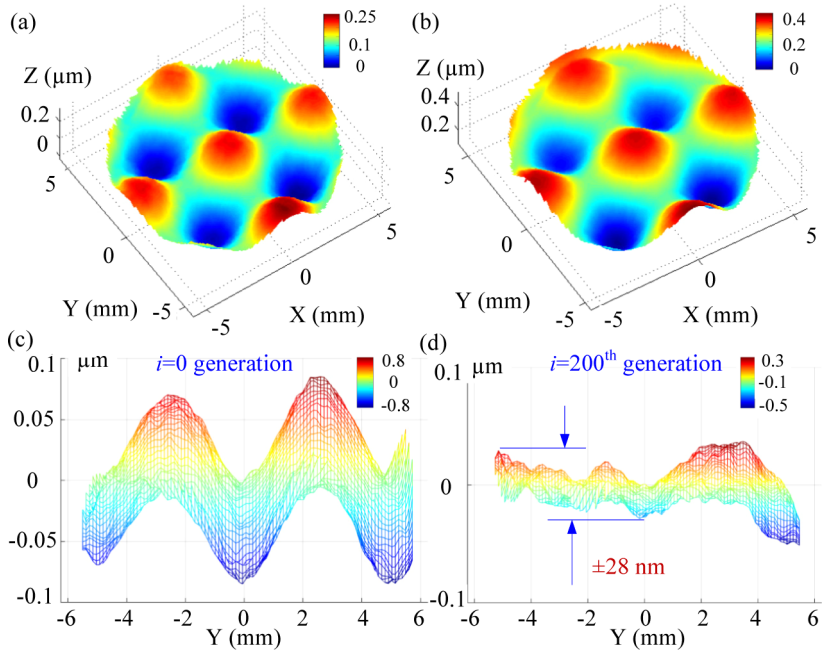

Fig. 12. Fabricated bi-sinusoidal freeform optical surfaces by (a) *VRR* method before optimization, (b) new approach, and residual errors by (c) *VRR* method before optimization, (d) new approach.

Optics EXPRESS

by an open loop in this study. Better performance is expected if the DFJ is controlled by a closed-loop system [29]. In addition, optical surface quality on the BK7 glass was obtained with final roughness of 2.6 nm ± 0.14 nm.

Furthermore, to validate the performance of proposed method when applied to freeform surfaces with larger amplitude, a bi-sinusoidal surface with 1.5 μm in PV was designed and fabricated. Using the same measurement methodology, the obtained surface form is drawn in Fig. 13(a), showing a good sinusoidal freeform surface. The side view in XZ plane is shown in Fig. 13(b). By registration with the designed surface, the form error is shown in Fig. 13(c) in the same range for comparison with the designed amplitude. Through the enlarged view in the inset of Fig. 13(c), the residual PV error is found to be well controlled within ± 55 nm, with an RMS error of 19 nm for the entire surface.

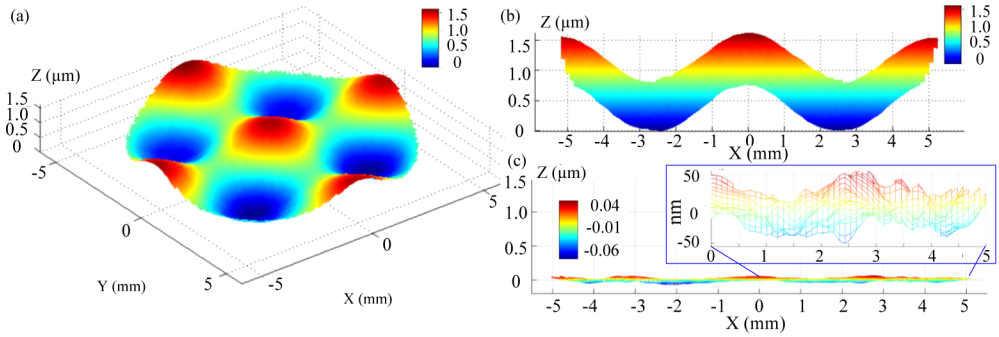

Fig. 13. (a) Fabricated bi-sinusoidal freeform optical surfaces with 1.5 μm in PV by new approach, (b) side view in XZ plane, (c) residual error compared to the design surface.

5. Summary

In this paper, a new approach for mapping the optimum dwell time was presented that enables ultra-precise generation of freeform optics by deterministic fluid jet (DFJ) fabrication. Zernike polynomials were innovatively utilized in the fabrication planning stage to construct the optimum dwell time map and show high potential in fabrication of accurate freeform optics. The residual error is remarkably reduced compared with the traditional volumetric removal rate (VRR) based method. Owing to the inherently smooth and continuous properties of Zernike polynomials over the entire target surface, the optimum dwell mapping is smooth with regard to feed motion of the machine. Besides, the new approach does not generate the large residual error at the edge region associated with the conventional iterative methods. Following some process investigation, experimental validation was conducted by fabricating typical freeform bi-sinusoidal optics. Benefiting from the new approach, residual error of the freeform surface was significantly lowered down to sub-100 nm in peak-to-valley value, with a final surface roughness of 2.6 nm on optical BK7 glass. It is noteworthy that the proposed methodology is not limited to DFJ process, but also potentially applicable to other deterministic time-dependent fabrication processes such as additive manufacture of optical components.

Funding

Japan Society for the Promotion of Science (17K14571).

Acknowledgments

We thank the grant program for research and development from the Mazak foundation, and acknowledge support from Zeeko Ltd. in loaning the machine and fluid jet system.

Optics EXPRESS

References

1. F. Fang, X. Zhang, A. Weckenmann, G. Zhang, and C. Evans, "Manufacturing and measurement of freeform optics," CIRP Ann. **62**(2), 823–846 (2013).
2. Z. Zhu, X. Zhou, D. Luo, and Q. Liu, "Development of pseudo-random diamond turning method for fabricating freeform optics with scattering homogenization," Opt. Express **21**(23), 28469–28482 (2013).
3. R. Mittal, R. K. Singh, and S. S. Joshi, "Elastohydrodynamic lubrication modeling of hydrodynamic nanopolishing process," J. Manuf. Sci. Eng. **134**(4), 041001 (2012).
4. D. Wang, H. Hu, L. Li, Y. Bai, X. Luo, D. Xue, and X. Zhang, "Effects of the gap slope on the distribution of removal rate in Belt-MRF," Opt. Express **25**(22), 26600–26614 (2017).
5. Y. Mori, K. Yamauchi, and K. Endo, "Elastic emission machining," Precis. Eng. **9**(3), 123–128 (1987).
6. O. W. Fähnle and H. H. van Brug, "Fluid jet polishing: removal process analysis," in *Optical Fabrication and Testing*, International Society for Optics and Photonics (1999) pp. 68–78.
7. D. D. Walker, D. Brooks, A. King, R. Freeman, R. Morton, G. McCavana, and S.-W. Kim, "The 'Precessions' tooling for polishing and figuring flat, spherical and aspheric surfaces," Opt. Express **11**(8), 958–964 (2003).
8. A. Beaucamp, T. Katsuura, and Z. Kawara, "A novel ultrasonic cavitation assisted fluid jet polishing system," CIRP Ann. **66**(1), 301–304 (2017).
9. C. Cheung, C. Wang, Z. Cao, L. Ho, and M. Liu, "Development of a multi-jet polishing process for inner surface finishing," Precis. Eng. **52**, 112–121 (2018).
10. A. Beaucamp and Y. Namba, "Super-smooth finishing of diamond turned hard X-ray molding dies by combined fluid jet and bonnet polishing," CIRP Ann. **62**(1), 315–318 (2013).
11. H. Li, W. Zhang, and G. Yu, "Study of weighted space deconvolution algorithm in computer controlled optical surfacing formation," Chin. Opt. Lett. **7**(7), 627–631 (2009).
12. R. A. Jones, "Optimization of computer controlled polishing," Appl. Opt. **16**(1), 218–224 (1977).
13. L. N. Allen and R. E. Keim, "An ion figuring system for large optic fabrication," in *Current Developments in Optical Engineering and Commercial Optics*, International Society for Optics and Photonics (1989) pp. 33–51.
14. C. Wang, W. Yang, Z. Wang, X. Yang, C. Hu, B. Zhong, Y. Guo, and Q. Xu, "Dwell-time algorithm for polishing large optics," Appl. Opt. **53**(21), 4752–4760 (2014).
15. S. Wilson and J. McNeil, "Neutral ion beam figuring of large optical surfaces," in *Current Developments in Optical Engineering II*, International Society for Optics and Photonics (1987) pp. 320–325.
16. C. L. Carnal, C. M. Egert, and K. W. Hylton, "Advanced matrix-based algorithm for ion-beam milling of optical components," in *Current Developments in Optical Design and Optical Engineering II*, International Society for Optics and Photonics (1992) pp. 54–63.
17. Z. Dong, H. Cheng, and H.-Y. Tam, "Robust linear equation dwell time model compatible with large scale discrete surface error matrix," Appl. Opt. **54**(10), 2747–2756 (2015).
18. W.-J. Deng, L.-G. Zheng, Y.-L. Shi, X.-K. Wang, and X.-J. Zhang, "Dwell-time algorithm based on matrix algebra and regularization method," Opt. Precis. Eng. **15**, 1009–1015 (2007).
19. J. F. Wu, Z. W. Lu, H. X. Zhang, and T. S. Wang, "Dwell time algorithm in ion beam figuring," Appl. Opt. **48**(20), 3930–3937 (2009).
20. L. Lu, L. Zhang, S. Ji, Y. Han, and J. Zhao, "An offline predictive feedrate scheduling method for parametric interpolation considering the constraints in trajectory and drive systems," Int. J. Adv. Des. Manuf. Technol. **83**(9-12), 2143–2157 (2016).
21. A. Bauer, E. M. Schiesser, and J. P. Rolland, "Starting geometry creation and design method for freeform optics," Nat. Commun. **9**(1), 1756 (2018).
22. D. R. Ibañez, J. A. Gomez-Pedrero, J. Alonso, and J. A. Quiroga, "Robust fitting of Zernike polynomials to noisy point clouds defined over connected domains of arbitrary shape," Opt. Express **24**(6), 5918–5933 (2016).
23. Z.-C. Cao, C. F. Cheung, and M. Y. Liu, "Model-based self-optimization method for form correction in the computer controlled bonnet polishing of optical freeform surfaces," Opt. Express **26**(2), 2065–2078 (2018).
24. L. N. Thibos, R. A. Applegate, J. T. Schwiegerling, and R. Webb, "Standards for reporting the optical aberrations of eyes," J. Refract. Surg. **18**, S652–S660 (2002).
25. Z. Zhu, X. Zhou, Q. Liu, and S. Zhao, "Multi-objective optimum design of fast tool servo based on improved differential evolution algorithm," J. Mech. Sci. Technol. **25**(12), 3141–3149 (2011).
26. K. Takizawa and A. Beaucamp, "Comparison of tool feed influence in CNC polishing between a novel circular-random path and other pseudo-random paths," Opt. Express **25**(19), 22411–22424 (2017).
27. W. Gao, S. Dejima, Y. Shimizu, S. Kiyono, and H. Yoshikawa, "Precision measurement of two-axis positions and tilt motions using a surface encoder," CIRP Ann. **52**(1), 435–438 (2003).
28. C. J. Evans, "Uncertainty evaluation for measurements of peak-to-valley surface form errors," CIRP Ann. **57**(1), 509–512 (2008).
29. A. Beaucamp, Y. Namba, and R. Freeman, "Dynamic multiphase modeling and optimization of fluid jet polishing process," CIRP Ann. **61**(1), 315–318 (2012).